

Energy-Efficient Activity Recognition Framework using Wearable Accelerometers

Atis Elsts^{a,b,*}, Niall Twomey^b, Ryan McConville^b, Ian Craddock^b

^a*Institute of Electronics and Computer Science, 14 Dzerbenes St., LV-1006, Riga, Latvia*

^b*Department of Electrical and Electronic Engineering, University of Bristol, 1 Cathedral Square, Bristol, BS15DD, UK*

Abstract

Acceleration data for activity recognition typically are collected on battery-powered devices, leading to a trade-off between high-accuracy recognition and energy-efficient operation. We investigate this trade-off from a feature selection perspective, and propose an energy-efficient activity recognition framework with two key components: a detailed energy consumption model and a number of feature selection algorithms. We evaluate the model and the algorithms using Random Forest classifiers to quantify the recognition accuracy, and find that the multi-objective Particle Swarm Optimization algorithm achieves the best results for the task. The results show that by selecting appropriate groups of features, energy consumption for computation and data transmission is reduced by an order of magnitude compared with the raw-data approach, and that the framework presents a flexible selection of feature groups that allow the designer to choose an appropriate accuracy-energy trade-off for a specific target application.

Key words: feature selection, activity recognition, wearables

1. Introduction

Internet of Things (IoT) networks and applications have gained tremendous popularity in the recent years [1, 2]. This includes applications of wearable devices [3].

*Corresponding author

Email addresses: `atis.elsts@edi.lv` (Atis Elsts)

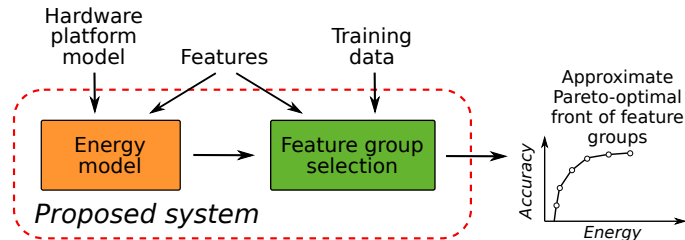


Figure 1: Overview of the proposed system.

5 Acceleration data from wearable devices are widely used for human activ-
 6 ity recognition applications in healthcare [4, 5], fitness [6], long-term behavior
 7 monitoring [7] and other areas. Their typical application uses a multistage
 8 process: after segmenting and filtering the raw sensor data, a number of sta-
 9 tistical features are computed and then used as inputs for a machine learning
 10 classifier. Wearable devices are battery powered; they have limited energy
 11 budgets, and the balance between high accuracy and energy-efficient opera-
 12 tion is important.

13 Wearable-based behavior monitoring studies often require a prolonged
 14 collection of data. Many commercial wearables require frequent recharging,
 15 but activity recognition systems for clinical or research purposes may not
 16 have the luxury of users that conform to a strict and cumbersome device-
 17 charging schedule. For elderly or ill people, the requirement to frequently
 18 recharge their devices may even be unethical. It is natural for designers of
 19 human activity recognition systems to ask these key questions:

- 20 • Given a specific target activity recognition accuracy, for what maximum
 21 time wearables can be deployed before they need to be recharged?
- 22 • Given a specific target deployment time, what is the maximum accuracy
 23 obtainable without recharging wearables during the deployment?

24 **Contributions.** This paper proposes a system (Fig. 1) that helps to be
 25 answer these questions. It is a framework for finding groups of features that
 26 have approximately optimal energy-accuracy trade-offs for a specific target
 27 application (i.e., classification of human activities of daily living) on a specific
 28 target platform. The framework consists of an energy model that describes
 29 the energy costs of feature extractions and transmissions together with a
 30 feature selection algorithm that optimizes both for accuracy and energy ef-
 31 ficiency. It uses training data collected from a previous study or from pilot
 32 experiments, a set of candidate platform, and a hardware platform model as

33 inputs, and produces the approximate Pareto-optimal front of non-dominated
 34 feature groups as the output. Our specific contributions are:

- 35 • We present a novel feature energy model that accounts for inter-dependencies
 36 between features to better estimate the energy consumption in
 37 the feature extraction process.
- 38 • We evaluate a number of feature group selection algorithms for the
 39 application domain.
- 40 • We present evidence about the suitability of the Particle Swarm Op-
 41 timization (PSO) algorithm, which we implement it in two different
 42 versions: as a multi-objective and as a single-objective optimization
 43 problem.

44 **Prototype system and results.** This paper assumes a setup where
 45 the sampling, preprocessing and feature extraction are done on the device,
 46 and the resulting features are wirelessly transmitted to a central system. We
 47 implement a C library for on-board feature extraction, run it on an ARM
 48 Cortex-M3 device, and measure the feature extraction time to estimate en-
 49 ergy consumption. The energy consumption model as well as three different
 50 datasets are used as inputs to the feature group selection algorithms. The
 51 evaluation scores the results in two dimensions: first, charge consumption
 52 for feature computation and transmission; second, the F_1 score for activity
 53 recognition. It compares the Pareto-optimal fronts selected by the PSO al-
 54 gorithms with those selected by methods from our previous work [8]: greedy
 55 search and mutual information (MI) based search. We evaluate the proposed
 56 system for classification of human activities of daily living with a Random
 57 Forest classifier, and compare the accuracy of the PSO algorithms with our
 58 previous work [8]. The PSO algorithms produce results that are closer to
 59 optimum than the alternatives, and the multi-objective PSO also finds the
 60 highest number of points on the front. The feature selection is assumed to
 61 be done offline, before the deployment of the data collection and feature ex-
 62 traction code, so that after running the feature group selection algorithms the
 63 desired features can be directly encoded in the deployed software.

64 Compared with our previous work [8] the present research adds selection
 65 of feature groups instead of merely evaluating individual features. We extend
 66 the feature extraction code from [8] with feature groups, several new features,
 67 and generic transforms and filters. Furthermore, we add the complete energy
 68 model, and describe how the system can be used to construct a practical
 69 feature extraction framework.

70 **Summary of the paper.** The paper first surveys the related work (Sec-
 71 tion [2](#)). Subsequently it presents the energy model (Section [3](#)) and the feature
 72 group selection algorithms (Section [4](#)). The evaluation of the framework is
 73 given in Section [5](#), and application examples in Section [6](#). Finally, the paper
 74 ends with conclusions (Section [7](#)).

75 Nomenclature

76 F_1 Precision and recall based measure of a test's accuracy

77 BLE Bluetooth Low Energy

78 CBOR Concise Binary Object Representation

79 HAR Human Activity Recognition

80 IoT Internet of Things

81 MI Mutual Information

82 BAMAP Physical Activity Monitoring for Aging People

83 PSO Particle Swarm Optimization

84 RF Random Forest

85 SMA Signal Magnitude Area

86 SBHERE Sensor Platform for Healthcare in a Residential Environment

87 SPW-2 SPHERE Wearable 2

88 UCI University California Irvine

89 2. Related Work

90 **Activity Recognition.** Accelerometer is a core sensor for human activ-
 91 ity recognition [9](#), [10](#). Even though the recognition accuracy can be improved
 92 by using multiple accelerometers at different locations on the body, good re-
 93 sults for coarse-grained activities can be obtained just from a single, typically
 94 wrist-worn device [11](#) – a setup that we assume in this paper.

95 Activity detection using deep learning can achieve state-of-the-art accu-
 96 racy [12]. However, deep learning is not suitable for the ultra-low energy
 97 consumption Class-1 IoT devices [13] our system targets; instead, it typi-
 98 cally targets smartphone-class devices [14] and beyond. The work by Lane *et*
 99 *al.* on deep learning for ARM Cortex-M is one exception from this trend;
 100 however, they admit that “work remains to make deep models of this scale
 101 completely practical” as they cannot be executed in real time [15].

102 **Energy Efficiency in Activity Recognition.** Energy efficiency has
 103 been a major research goal for the community, as well as a driver for Edge
 104 Computing – the trend where computation moves away from the cloud and
 105 closer to the data-producing devices [16]. Our work is an instance of the
 106 Edge Computing paradigm.

107 In most of the related work, the accuracy-energy trade-off is not explicitly
 108 defined; rather, the strategy is to achieve subjectively “good-enough” accu-
 109 racy while optimizing the energy usage [17, 18, 19]. As a result the minimal
 110 accuracy threshold is hidden in the details in the proposed systems. By be-
 111 ing explicit and not forcing a single threshold value, our work achieves better
 112 transparency and flexibility.

113 Yan *et al.* [17] propose to optimize sampling rate and classification fea-
 114 tures on mobile phones separately for each activity, in a real-time, adaptive
 115 fashion. The system proposed in our paper can be applied to select the fea-
 116 tures for a single, specific activity or a subgroup of activities, serving as a
 117 building block in their approach.

118 Another approach is to decide which sensors can be turned off without
 119 losing a lot accuracy. Gordon *et al.* [18] optimize sensor usage based on
 120 prediction of future activities. Similarly, in case of multiple sensor devices,
 121 some of them can be delegated to “backup” status, thus saving the energy
 122 spent by the whole system [20]. Again, these approaches can complement
 123 the feature-selection system of this paper. Trivially, a sensor can be turned
 124 off if no features use the data produced by this sensor; the energy saved by
 125 that would be captured by the platform’s energy model.

126 Hierarchical activity recognition is another natural extension. For exam-
 127 ple, Liang *et al.* [19] propose a hierarchical recognition algorithm that only
 128 computes the more expensive frequency domain features when the activity
 129 cannot be reliably classified by time domain features. Zheng *et al.* [21] show
 130 that a hierarchical classifier allows to reduce the sampling frequency several
 131 times while maintaining “high accuracy”. Hierarchical classifiers are be-
 132 yond the scope of the present paper, however, we aim to generalize the results

133 for this in our future work.

134 **Feature Extraction.** In terms of feature extraction on low-power em-
 135 bedded devices, we build on our previous work [8]. We extend the work by
 136 adding the notion of generalized transforms in the feature extraction stage.
 137 We also add a number of new features, and drop those features that showed
 138 bad energy-accuracy trade-off in our previous work.

139 **Feature Selection.** We build on the extensive existing work in feature
 140 selection [22] and experiment with both wrapper and filter methods [23].
 141 The particle swarm optimization method [24] has been previously proposed
 142 for feature selection [25]. That includes the multi-objective optimization
 143 that relies on nondominated sorting [26]. However, the energy costs of the
 144 recognition are typically not quantified in detail; frequently, existing works
 145 use the number of features as a proxy for cost (i.e., energy consumption);
 146 see [27, 28] for examples. In this paper, we provide a detailed energy model
 147 for computing the cost of feature groups.

148 **Accuracy-Energy Trade-Offs.** One typical way to investigate the
 149 trade-off for the target application is to compare off-node and on-node ac-
 150 tivity recognition schemes [29]. Our work falls in between these two extreme
 151 approaches: while the recognition is done off-node, the software on the node
 152 is optimized in an application-specific way to extract only the features that
 153 are required by the application.

154 Chu *et al.* propose a system for multi-objective optimization of mobile
 155 sensor classifiers [30]; while the Pareto-optimal offline optimization approach
 156 is the same as used in our paper, we operate at the level of feature groups,
 157 rather than classifiers. Similarly, Jensen *et al.* propose a method for ap-
 158 proaching the accuracy-cost conflict by choosing an appropriate classifier [31];
 159 however, they ignore the feature selection step, as well as abstract away from
 160 the target hardware instead of using an empirical energy model.

161 3. Energy Model

162 3.1. Features, Transforms, and Filters

163 Let us denote the vector of the raw samples with $\mathbf{s} = (s_1, s_2, \dots, s_n)$,
 164 where $s_i \in \mathbb{R}$. Normally, acceleration data is three dimensional, i.e., there are
 165 three vectors $\mathbf{s}_x = (x_1, x_2, \dots, x_n)$, $\mathbf{s}_y = (y_1, y_2, \dots, y_n)$, $\mathbf{s}_z = (z_1, z_2, \dots, z_n)$
 166 corresponding to acceleration in the three spatial dimensions.

167 In a preprocessing stage, the data is segmented in windows. Assuming
 168 window size w and processing interval k , the j -th window of the input data

169 is the vector $W(s)_j = (s_{j \cdot k}, s_{j \cdot k + 1}, \dots, s_{j \cdot k + w - 1})$. If $k < w$, the neighboring
 170 windows overlap each another.

171 *Features, transforms and filters* are functions that act on the raw data,
 172 either on a single dimension separately or the vector of the three spatial
 173 dimensions. The difference between a them is that a feature f is calculated
 174 once per window ($f : \mathbb{R}^w \rightarrow \mathbb{R}$ or $f : \mathbb{R}^{3w} \rightarrow \mathbb{R}$), while a transform or a filter
 175 t creates an output value for every input value ($t : \mathbb{R} \rightarrow \mathbb{R}$ or $t : \mathbb{R}^3 \rightarrow \mathbb{R}$).
 176 The difference between the transform and a filter is that a transform does
 177 not lose information and is reversible. For simplicity, in some occasions in
 178 this paper we use the term “transform” to denote any function that conforms
 179 to the output value criteria above.

180 3.2. Feature Preselection

181 The list of candidate features is given in Table 1. We also introduce a
 182 number of *transforms and filters* (Table 2) that preprocess the data before the
 183 feature extraction. For example, transforming the data with the *magnitude*
 184 *squared* function makes it more robust to rotations of the wearable compared
 185 with computing features of each axis separately. (Note that the list does not
 186 include the *magnitude* filter. It was deemed too expensive, since it requires
 187 to compute a square root operation for each (x_i, y_i, z_i) sample.) All data is
 188 first passed to a median-of-three filter to de-noise it. This filter is assumed to
 189 be always enabled, and as such not handled by the group selection process.

Table 1: Features.

Feature	Definition
Mean	$\mu_s = \frac{1}{w} \sum_{i=1}^w s_i$
Minimum	$\min(s)$
Maximum	$\max(s)$
First Quartile	$\text{sorted}(s)_{w/4}$
Median	$\text{sorted}(s)_{w/2}$
Third Quartile	$\text{sorted}(s)_{3w/4}$
Inter-quartile range	$\text{sorted}(s)_{3w/4} - \text{sorted}(s)_{w/4}$
Energy	$E_s = \frac{1}{w} \sum_{i=1}^w (s_i)^2$
Standard Deviation	$\sqrt{E_s - (\mu_s)^2}$
Correlation	$C(\mathbf{s}_u, \mathbf{s}_v) = \frac{\sum_{i=1}^w (u_i - \mu_u)(v_i - \mu_v)}{\sqrt{\sum_{i=1}^w (u_i - \mu_u)^2 \sum_{i=1}^w (v_i - \mu_v)^2}}$
Entropy	$-\sum_{i=1}^w P(s_i) \log P(s_i)$

Table 2: Transforms and filters.

Transform/Filter	Definition
Median-of-three	$\text{median}(s_{i-1}, s_i, s_{i+1})$
Jerk	$s_i - s_{i-1}$
L1 norm	$\text{abs}(x_i) + \text{abs}(y_i) + \text{abs}(z_i)$
Magnitude squared	$x_i^2 + y_i^2 + z_i^2$

190 The results in [8] show that for recognition of a limited set of coarse-
 191 grained activities of daily living (such as walking, standing, sitting, and ly-
 192 ing) simple time-domain features have the best energy-accuracy trade-offs.
 193 Inspired by those results, we only use time-domain features for this paper,
 194 eschewing the need to run the Fourier transform or other similar transforms
 195 on the device to obtain frequency-domain features. To make it clear, this

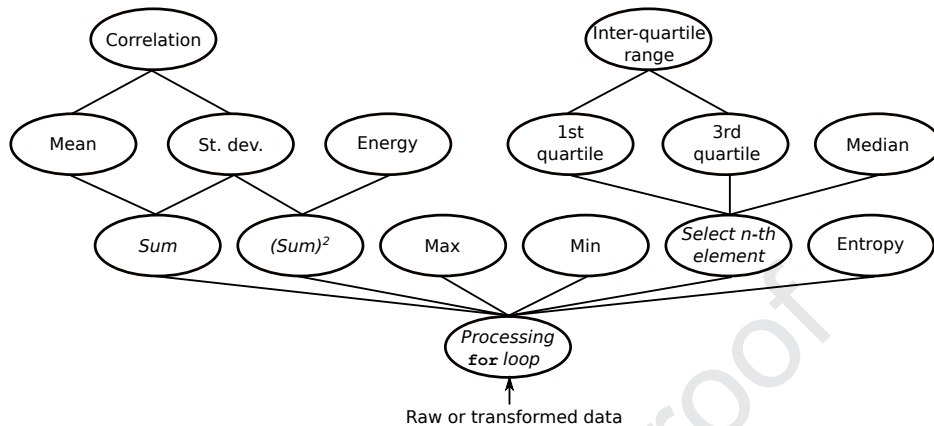


Figure 2: Features under consideration and their inter-dependencies. Labeled in *italics*: intermediate results that are included in the energy model, but not in the feature group selection stage.

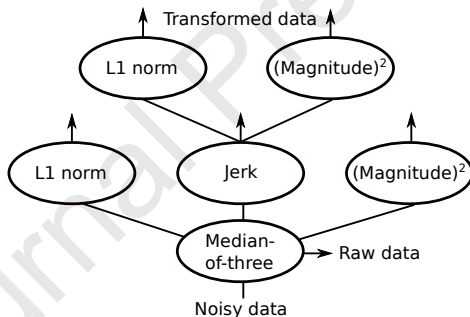


Figure 3: Transforms and filters applied to the raw data.

196 pre-selection is done because of pragmatic reasons; the approach described
 197 further in this paper is not limited to the specific functions we are using.

198 Floating-point arithmetic is used to compute the *standard deviation*, *cor-*
 199 *relation* between axis, *energy* and *entropy*. The remaining features, including
 200 the *mean*, use only fixed-point arithmetic.

201 We note that the final list of features includes time domain features typi-
 202 cally used in published research in this field, even if occasionally under differ-
 203 ent names. For example, the “ κ feature” defined and used by Wang *et al.* [29]
 204 is included implicitly: as mean computed on the *jerk*-transformed data in
 205 its normalized version. The *Signal Magnitude Area (SMA)* feature [9] is also
 206 included implicitly, as the mean computed on the L1 norm.

207 In further analysis, we assume that all features are computed on all three

208 axis (x, y, z) of acceleration data, where applicable. The inter-axis correla-
 209 tion feature is computed for all three pairs of axis $(xy, xy$ and $yz)$.

210 3.3. Energy Costs

211 Let us define the *cost* of \mathbf{f} , where \mathbf{f} is a function that is either a feature
 212 or a transform, as the energy needed to iteratively compute the function on
 213 a single window W of samples ($W \in \mathbb{R}^{3w}$ or $W \in \mathbb{R}^w$).

214 Features and transforms can be combined; for example, one can first
 215 transform the data using the *jerk* transform, then transform the result using
 216 the *magnitude squared* transform, then segment the data and calculate the
 217 standard deviation of each segment. More generally, the combinations of
 218 any two different transforms t_i and t_j yields two new transforms $t_i(t_j(s))$ and
 219 $t_j(t_i(s))$ in our model. Similarly, any transform t can be combined with any
 220 feature f to yield a new feature $f(t(s))$.

221 Multiple features cannot be combined in this general way; however, one
 222 can notice that there are directional dependencies between some of the fea-
 223 tures. For example, to calculate the standard deviation, one must calculate
 224 the mean. Therefore if both the standard deviation and the mean are in-
 225 cluded in a group of features, then their total calculation cost is equal to
 226 the calculation cost of the standard deviation, not the sum of the costs of
 227 these two individual features. In Section 3.4 we describe such an optimized
 228 implementation, and use it further in the paper.

229 More generally, if f_1 and f_2 are features that both use an intermediate
 230 result \mathbf{g} , where \mathbf{g} is either a feature or a transform, then the cumulative cost
 231 of the feature set $\{f_1, f_2\}$ is:

$$cost(\{f_1, f_2\}) = cost(f_1) + cost(f_2) - cost(\mathbf{g}) \quad (1)$$

232 In the special case when the intermediate result \mathbf{g} is equal to one of the
 233 features f_1 or f_2 :

$$cost(\{f_1, f_2\}) = max(cost(f_1), cost(f_2)) \quad (2)$$

234 Let us generalize Eq. 1. First, let us assume that the energy cost of a set
 235 $\{f_1, \dots, f_m\}$ of features and transform is already known and equal to c_m , and
 236 that the task is to add a new feature f_{m+1} to this set that uses some inter-
 237 mediate result \mathbf{g} that is already computed. Then the cost of the combined
 238 set is:

$$c_{m+1} = cost(\{f_1, \dots, f_{m+1}\}) = c_m + cost(f_{m+1}) - cost(\mathbf{g}). \quad (3)$$

239 This approach is used to iteratively compute the cost of a set of features
 240 using their individual costs (Section 3.5) for the target hardware platform
 241 (Section 3.4) using the dependencies shown in Figs. 2 and 3.

242 3.4. Example Hardware Platform

243 3.4.1. Platform Description

244 We evaluate the cost of the on-board feature extraction on SPW-2 [32]
 245 (Fig. 4), an embedded hardware platform based on ARM 32-bit Cortex-
 246 M3 core. Its limited RAM and program memory size (20 kB and 128 kB,
 247 respectively) and CPU speed (48 MHz) do not allow to run high-complexity
 248 algorithms. However, the System-on-Chip has a 2.4 GHz ultra-low power
 249 wireless radio for data transmission.



Figure 4: SPW-2: ARM Cortex-M3 based wearable accelerometer platform [32].

250 3.4.2. Computation

251 We implement the feature extraction as a stand-alone library¹. The li-
 252 brary is written in C programming language; the code is fully compatible
 253 with the C99 language standard and portable, as it does not contain any
 254 ARM Cortex specific functionality. To approximate the energy cost of com-
 255 puting each feature, we experimentally evaluate it on the SPW-2. To achieve
 256 that, the library is linked with the Contiki-NG operating system².

257 The evaluation of the library consists of performance measurements of
 258 15 000 samples of real 3-axial acceleration data samples, taken from the
 259 SPHERE Challenge dataset. For each function, we measure the time it
 260 takes to segment the samples in 128-sample windows with 50% overlap and
 261 compute that feature for each window. This window size and overlap has
 262 been shown to give good results in previous research [9, 10].

¹Available at <https://github.com/atiselsts/feature-group-selection>

²<http://contiki-ng.org/>

263 The evaluation results consist of timing measurements that capture the
 264 time required to compute each feature. The features are computed on data
 265 that is scaled to the range of 8-bit signed integer. As the active-mode current
 266 consumption of the SPW-2 platform [32] is constant, the time taken for the
 267 computation accurately corresponds to the charge consumption of the micro-
 268 controller. We use the electric charge as the main metric, rather than energy
 269 (charge times voltage). The CC2650 System-on-Chip has high dynamic range
 270 of voltage (from 1.8 to 3.8 V); the exact number is a platform-specific value
 271 not relevant to the optimization goals of this paper.

272 The C library contains both the implementation of individual features and
 273 the implementation of feature groups, such as the group $\{mean, standard$
 274 $deviation\}$. The latter is implemented separately, as a group. It is more
 275 efficient that way since these features are interdependent. Specifically, both
 276 features require the computation of the sum of samples in each window. The
 277 inter-dependencies from Fig. 2 are used to decide which feature groups to
 278 implement in this combined way.

279 Note that each feature requires to process the data in a `for` loop. We
 280 assume that in an optimized implementation to extract a specific group of
 281 N features, there would be just one `for` loop. To accurately evaluate the
 282 cumulative charge consumption of this group from our experimental data,
 283 we need to sum their individual costs and then subtract the cost of the
 284 empty `for` loop multiplied by $N - 1$ (see Eq. 3).

285 3.4.3. Data Transmission

286 The CC2650 System-on-Chip supports two radio modes: BLE (Bluetooth
 287 Low Energy) and IEEE 802.15.4. As a result, we select IEEE 802.15.4 for
 288 our transmission model.

289 We use a model that assumes a 50% overhead. That is, the model assumes
 290 that in order to transmit one byte of application-layer payload, two bytes
 291 need to be transmitted in total. This accounts for packet header overhead,
 292 for ACKs, and for occasional retransmissions of complete packets.

293 To calculate the amount of the application data to transmit, the results
 294 of the feature extraction algorithm are encoded in an efficient way. For
 295 integers, CBOR [33] encoding is used, while for floating point numbers: their
 296 size reduced to 16 bits. Finally, to estimate the charge consumption, we
 297 measured the transmission-mode current of the target platform. When the
 298 transmission output power is set to 5 dBm, it is approximately 12.0 mA.

Table 3: Charge consumption for feature extraction on the SPW-2 wearable platform.

Feature / transform / filter	Cost (per 128 sample window)	CPU time	Avg. current (at 50 Hz)
Mean	0.026 μC	6.8 μs	0.067 μA
Minimum	0.026 μC	6.8 μs	0.067 μA
Maximum	0.026 μC	6.8 μs	0.067 μA
First quartile	0.064 μC	16.8 μs	0.165 μA
Median	0.064 μC	16.8 μs	0.165 μA
Third quartile	0.064 μC	16.8 μs	0.165 μA
Inter-quartile range	0.070 μC	18.2 μs	0.179 μA
Energy	0.032 μC	8.4 μs	0.083 μA
Standard deviation	0.035 μC	9.2 μs	0.090 μA
Correlation	0.067 μC	17.3 μs	0.170 μA
Entropy	0.257 μC	66.9 μs	0.659 μA
Median-of-three	0.033 μC	8.6 μs	0.085 μA
L1 norm	0.034 μC	8.9 μs	0.088 μA
Magnitude squared	0.029 μC	7.6 μs	0.075 μA
Jerk + L1 norm	0.047 μC	12.2 μs	0.120 μA
Jerk + Magnitude sq.	0.048 μC	12.5 μs	0.123 μA
Empty for loop	0.010 μC	3.2 μs	0.032 μA

Table 4: Charge consumption for transmission on the SPW-2 wearable platform.

Feature	Cost per window (128 samples)	Avg. current (at 50 Hz)
Mean	0.89 μC	2.29 μA
Minimum	1.02 μC	2.60 μA
Maximum	1.17 μC	3.00 μA
First quartile	1.02 μC	2.60 μA
Median	1.02 μC	2.60 μA
Third quartile	1.02 μC	2.60 μA
Inter-quartile range	0.84 μC	2.16 μA
Energy	1.49 μC	3.81 μA
Standard deviation	1.49 μC	3.81 μA
Correlation	1.49 μC	3.81 μA
Entropy	1.49 μC	3.81 μA
Raw data	31.46 μC	80.54 μA

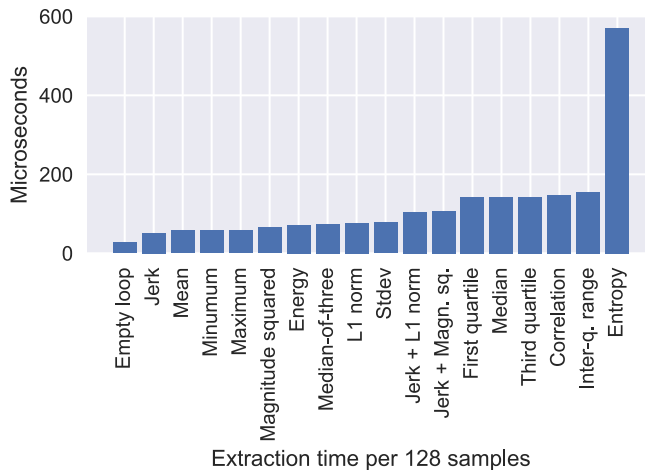


Figure 5: Extraction time for features and transforms.

3.5. Model Instantiation for the Example Hardware Platform

Table 3 and Table 4 show the instantiation of the charge consumption model. The Fig. 5 graphically displays the feature extraction time from the Table 3. The charge consumption costs are given for a single axis of acceleration data. In general, it is more than an order of magnitude cheaper to compute a feature than to transmit the result of the computation. The only exception is the *entropy* feature. Transmission of the raw data unsurprisingly is another order of magnitude more expensive, since it means sending 64 measurements per each window instead of sending just one value.

4. Feature Group Selection Methodology

4.1. Preliminaries

In contrast to single-objective optimization that optimizes over scalars, multi-objective optimizes over vector-valued functions. These optimization problems take the following general form:

$$\begin{aligned} \min & (f_1(\mathbf{x}), f_2(\mathbf{x}), \dots, f_k(\mathbf{x})) \\ \text{s.t. } & \mathbf{x} \in \mathcal{X}, \end{aligned}$$

in which the k functions to be optimized are denoted as f_i (with $1 \leq i \leq k$), and \mathcal{X} is the feasible set of solutions.

315 A key concept within multi-objective domain is that of dominant solu-
 316 tions. A solution $\mathbf{x}_1 \in \mathcal{X}$ is said to dominate another solution $\mathbf{x}_2 \in \mathcal{X}$ if:

- 317 1. $f_i(\mathbf{x}_1) \leq f_i(\mathbf{x}_2) \forall i (1 \leq i \leq k)$; and
- 318 2. $f_i(\mathbf{x}_1) < f_i(\mathbf{x}_2)$ at least once.

319 This important property means that \mathbf{x}_1 is never *worse* than \mathbf{x}_2 . If a solu-
 320 tion $\mathbf{x}_* \in \mathcal{X}$ dominates the set $\mathcal{X} \setminus \{\mathbf{x}_*\}$, then \mathbf{x}_* is said to be *Pareto optimal*.
 321 Pareto optimality is noteworthy since the performance of any single objec-
 322 tive at a Pareto optimal solution cannot be improved without compromising
 323 performance on the other objectives.

324 The set of Pareto optimal solutions is called the *Pareto front* and it es-
 325 tablishes the relationship between a set of Pareto optimal solutions and a set
 326 of operating contexts. In this work, the power budget for feature representa-
 327 tion calculation defines the operating context. In other words, with access to
 328 the Pareto front, feature representations can be adjusted depending on the
 329 power budget. Typically, the front will be calculated offline and deployed to
 330 the embedded device. The computational expense required to calculate the
 331 Pareto front is the primary reason for this, however, the resulting model is
 332 trivial to evaluate on embedded devices.

333 4.2. The Multi-Objective Optimization Problem

The optimization problem in the context of this work is defined as:

$$\text{minimize } (-a(\mathbf{f}), e(\mathbf{f})) \quad (4)$$

$$\text{subject to } \|\mathbf{f}\| > 0, \quad (5)$$

334 where \mathbf{f} is a set of feature vectors, $a(\mathbf{f})$ is the classification accuracy given \mathbf{f} ,
 335 and $e(\mathbf{f})$ is the energy cost to compute and transmit \mathbf{f} . The *solution* of this
 336 optimization problem is the Pareto front of k non-dominated sets of feature
 337 vectors $\mathbf{f}^{(1)}, \mathbf{f}^{(2)}, \dots, \mathbf{f}^{(k)}$. The *granularity* of the solution is the number k .

338 Within this work, we are concerned with two objectives (*i.e.* $k = 2$): high
 339 predictive accuracy, and low power consumption for data representation.
 340 Taking into account all features and their combinations with the different
 341 transforms (Section 3), there are 54 total feature vectors under considera-
 342 tion. Since the number of subsets in a 54-element set is very large, it is not
 343 possible to apply a brute force algorithm to find the nondominated subsets
 344 of feature vectors. If more features such as frequency domain features are

345 added, the need to reduce the computational complexity of the search be-
 346 comes even stronger. Note that some of the features are three-dimensional
 347 vectors, e.g., *mean*, when computed on a segment of the raw data, results in
 348 the triple (*mean_x*, *mean_y*, *mean_z*). If these were separated along the three
 349 axis, that would improve the granularity of the results, but also massively
 350 increase the number of the features and thus the search space.

351 4.3. Activity Recognition Classifier

352 We use the Random Forest classifier to evaluate the accuracy. The general
 353 approach described in this paper is not specific to any particular classifier;
 354 we selected the Random Forest because it is computationally inexpensive
 355 and robust, and has shown good results in a wide range of applications.
 356 Furthermore, the features do not need to be normalized when the Random
 357 Forest is used; this reduces the computation required for feature extraction.
 358 The classifier is implemented using the *scikit-learn* library. The number
 359 of trees is set to 100 (the default for version 0.22), and the `class_weight`
 360 parameter set to “balanced” to handle skewed class distributions.

361 4.4. Selection Algorithms

362 Feature selection methods are categorized in wrapper, filter, and embed-
 363 ded methods [23]. The first treats the problem as a black box, the second uses
 364 a pre-processing step independent of the classifier, and the third uses infor-
 365 mation specific to the classifier. We compare a number of wrapper methods:
 366 greedy search and PSO based search, as well as one filter method: mutual
 367 information based selection. In terms of embedded methods, the feature im-
 368 portances in the Random Forest is a potential candidate. However, the splits
 369 in the decision tree construction process are selected in a way that maximizes
 370 information gain. Therefore, the results of selecting by feature importances
 371 are going to be the same as when selecting by MI.

372 4.4.1. Greedy Search

373 The idea of the greedy search is to start with an empty set of selected
 374 features, and then add a single highest-scoring feature in each step. The
 375 performance of a candidate group of features \mathbf{f} is measured by training a
 376 Random Forest classifier on the training data and evaluating its accuracy on
 377 the validation data. The measurement score S linearly combines the F_1 score
 378 of this evaluation with the energy consumption E of the group \mathbf{f} :

$$S = W_E E + W_A F_1, \quad (6)$$

379 The weights W_A and W_E are selected to scale the accuracy and energy
 380 metrics to similar amplitude and the same direction: $W_A = -500 W_E$. En-
 381 ergy is a large number that needs to be minimized, and F_1 score needs to be
 382 maximized, subject to $0.0 \leq F_1 \leq 1.0$. Once a feature is selected, it is never
 383 removed from the set. See the Algorithm 1 for the details.

Algorithm 1 Greedy Search

```

max_cost ← energy_cost({raw_data})
selected_features ← ∅
score = −∞
pareto_front = list()
while true do
  best_candidate_score = −∞
  for  $f \in$  candidate_features do
    if  $f \notin$  selected_features then
      candidate_selection = selected_features ∪ {f}
      new_score ← evaluate_energy_and_f1score(candidate_selection)
      if new_score > best_candidate_score then
        best_candidate_score ← new_score
        best_candidate ← f
      end if
    end if
  end for
  selected_features ← selected_features ∪ {best_candidate}
  if energy_cost(selected_features) ≥ max_cost then
    break
  end if
  improvement ← best_candidate_score − score
  score ← best_candidate_score
  pareto_front.append(selected_features)
end while
return pareto_front

```

▷ Initialization

▷ Main loop

384 4.4.2. Mutual Information Based Selection

385 Mutual information (MI) is a statistical measure between two random
 386 variables X and Y that quantifies the reduction in uncertainty about one
 387 random variable given knowledge of another. High MI indicates a large
 388 reduction in uncertainty. Hence, MI measures the reduction in uncertainty
 389 about the classification target Y given a feature X . More formally, given

Algorithm 2 Mutual Information Based Selection

```

max_cost ← energy_cost({raw_data})
selected_features ← ∅
score = −∞
pareto_front = list()
MI_list = list()
while true do
  for f ∈ candidate_features do
    MI_list ← sort(calculate_MI(f, classes))
  end for
  for f ∈ MI_list do
    selected_features = selected_features ∪ {f}
    new_score ← evaluate_energy_and_f1score(selected_features)
  end for
  if energy_cost(selected_features) ≥ max_cost then
    break
  end if
  pareto_front.append(selected_features)
end while
return pareto_front

```

▷ Initialization

▷ Main loop

390 discrete random variables X and Y , the MI between them is:

$$I(X; Y) = \sum_{y \in \mathcal{Y}} \sum_{x \in \mathcal{X}} p(x, y) \log \left(\frac{p(x, y)}{p(x)p(y)} \right) \quad (7)$$

391 where $p(x, y)$ is the joint probability distribution function of X and Y , and
 392 $p(x)$ and $p(y)$ the marginal probability distribution functions of X and Y .

393 In the MI based selection, all features are initially ranked according to
 394 their MI with the classification target classes. Then, the highest ranking
 395 features are one-by-one added to the candidate set, until a predetermined
 396 number of features have been chosen (Algorithm 2). This is a filter based
 397 method; in contrast to the greedy search, it does not use information from
 398 classification results to guide the search.

399 4.4.3. Particle Swarm Optimization Based Search

400 The Particle Swarm Optimization (PSO) is a global stochastic optimiza-
 401 tion method. It uses a population of candidate solutions (particles). The
 402 *position* of a particle is defined as the n -dimensional vector describing the par-
 403 ticles coordinates in the search space. The *velocity* is another n -dimensional

404 vector describing the rate of change of the position. The PSO algorithm
 405 is iterative; in each iteration it updates the particles according to simple
 406 mathematical rules based on the particles' positions and velocities.

407 The PSO algorithm is a popular meta-heuristic method for solving non-
 408 linear optimization problems, including feature selection [25]. It is suitable
 409 for searching in a very large space of candidate solutions, and does not re-
 410 quire the optimization function to be differentiable. However, as with other
 411 stochastic optimization methods, PSO is not guaranteed to find the global
 412 optima. It may also take a long time to converge.

413 For the purposes of this paper, we define the search space as the power
 414 set of the candidate features. Elements of the particle's position vector can
 415 take values from 0.0 to 1.0. If the value of an position element x_i is greater
 416 than the THRESHOLD constant, the i -th feature is defined as *selected* by the
 417 particle; THRESHOLD = 0.9 in our implementation to bias the search towards
 418 sparser selections.

Table 5: PSO algorithm parameters (from [25]).

Parameter	Value
Maximum Iterations	100
Number of Particles	10 000
Inertia Weight	0.7298
Max Speed	0.6
Acceleration c_1	1.49618
Acceleration c_2	1.49618

419 We implement two versions of the PSO search:

- 420 • Single objective. Here the score S of a particle is a scalar, calculated
 421 as in the Eq. 6. The traditional PSO algorithm is used [34].
- 422 • Multi-objective. Here the score of a particle is 2-dimensional vector
 423 that includes the energy and F_1 score values as its elements. As tradi-
 424 tional PSO method cannot handle multi-objective optimization, we
 425 utilize the NSPSOFS algorithm by Xue *et al.* [25]. This algorithm relies
 426 on nondominated sorting [26] to produce the Pareto-optimal fronts in
 427 each iteration, and attempts to move the rest of the particles towards
 428 this front. In each iteration it also prunes the Pareto-optimal fronts by

429 sorting its particles by crowding (distance to neighbors) and removing
 430 25 % of the most overcrowded particles.

431 Algorithm 3 shows the details how the PSO methods are incorporated in
 432 the feature group selection process. Table 5 lists configuration parameters of
 433 the PSO algorithm; the weight, speed and acceleration parameters are taken
 434 from Xue *et al.* [25]. For a detailed explanation of the PSO algorithms, in
 435 particular the multi-objective version, we ask the reader to consult [25].

Algorithm 3 PSO Based Search

```

NUM_PARTICLES ← 10 000                                     ▷ Configuration constants

particles ← ∅                                             ▷ Initialization

for f1 ∈ candidate_features do
  for f2 ∈ candidate_features do
    if f1 ≠ f2 then
      p ← Particle()
      p.features ← list(f1, f2)
      particles ← particles ∪ {p}
    end if
  end for
end for

while length(particles) < NUM_PARTICLES do
  p ← Particle()
  p.features ← random_subset(candidate_features)
  particles ← particles ∪ {p}
end while

for p ∈ particles do
  p.score ← evaluate_energy_and_f1score(p.features)
end for

run_particle_swarm_optimization(particles)                ▷ Optimization

for p ∈ particles do
  p.score ← evaluate_energy_and_f1score(p.features)
end for

sorted_particle_sets ← nondominated_sort(particles)
pareto_front ← list(particle.features for particle ∈ sorted_particle_sets[0])
return pareto_front

```

436 4.5. Datasets

Table 6: Datasets used.

	PAMAP2 Dataset	HAR Dataset	SPHERE Challenge Dataset
Sampling rate	100 Hz	50 Hz	20 Hz
Number of activities	12	6	3
Number of windows	15 140	10 299	1160
Duration	5.4 h	7.3 h	2.1 h
Wearable position used	wrist	waist	wrist

437 The *PAMAP2 Dataset* [35] contains data of multiple physical activities
 438 performed by 9 subjects wearing 3 inertial measurement units (over the wrist
 439 on the dominant arm, on the chest, and on the dominant side’s ankle) and
 440 a heart rate monitor. In this paper, we use the data of their 12 “protocol”
 441 activities: lying, sitting, standing, ironing, vacuum cleaning, ascending stairs,
 442 descending stairs, walking, Nordic walking, running, and rope jumping. Data
 443 were sampled at 100 Hz in this work and we use only the accelerometer data,
 444 although magnetometer and gyroscope data are also available.

445 The *UCI HAR Dataset* [36] was collected by attaching a smart-phone
 446 (with accelerometer and gyroscope) in a waist-mounted holder, with 30 par-
 447 ticipants conducting 6 activities in a controlled laboratory environment. Six
 448 activities were annotated in this dataset: walking, walking up stairs, walking
 449 down stairs, sitting, standing, and lying down. The acceleration was sam-
 450 pled at 50 Hz on triaxial accelerometers and gyroscopes. Since gyroscopes
 451 can consume several orders of magnitude more power than accelerometers,
 452 we only assess the accelerometer data in our treatment of this work.

453 The *SPHERE Challenge Dataset* [37] contains synchronized accelerome-
 454 ter, environmental and video data that was recorded in a smart home by the
 455 SPHERE project [38, 7, 39]. Three sensing modalities were collected in this
 456 dataset: 1) environmental sensor data; 2) accelerometer and Received Signal
 457 Strength Indication data; and 3) video and depth data. Accompanying these
 458 data are annotations on location within the smart home, as well as anno-
 459 tations relating to the Activities of Daily Living that were being performed
 460 at the time. In this work we consider only the acceleration data. Twenty
 461 activities were annotated in this dataset, and 10 participants participated

462 volunteered for the challenge totaling approximately 9 hours of data. In or-
 463 der to avoid having to deal with missing data in this paper, we use a subset
 464 of the dataset: the activities of six participants, each of which has $< 5\%$ of
 465 samples missing because of lost over-the-air packets, and quantize the read-
 466 ings as 8-bit integers. Only three activities from this subset have sufficient
 467 amounts of data (>100 windows each), so we only use those three.

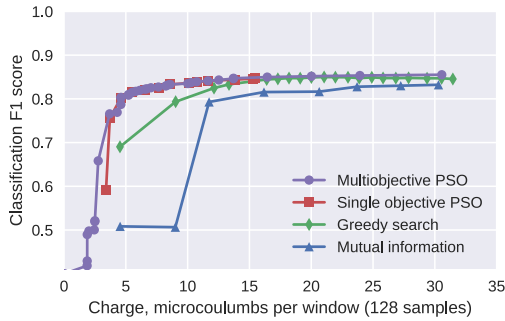
468 4.6. Feature Group Selection Algorithm

469 The feature group selection is done for each dataset independently using
 470 this process:

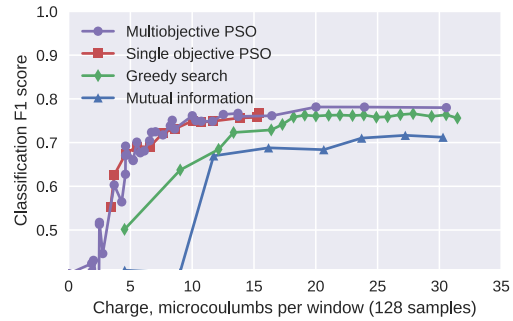
- 471 1. The raw data in the dataset is preprocessed: segmented in 128-sample
 472 windows (50% overlap).
- 473 2. To each of the segments, one activity value is assigned. If at least $2/3$
 474 of entries in that segment have a single activity the value is set to the
 475 dominant activity code during that segment; it is set to -1 otherwise.
- 476 3. All features are calculated for each window.
- 477 4. The features of a randomly selected subject are removed from the dataset.
- 478 5. Each feature selection algorithm is run using the features from the main
 479 dataset as inputs and F_1 scores from three-fold cross validation as the
 480 performance metric.
- 481 6. The performance on the subject-left-out is separately measured for each
 482 feature group. It is reported to show the generalizability of the results.

483 5. Results

484 The results (Figs. 6, 7, 8) show the expected shape of the approximate
 485 Pareto-optimal fronts. When the charge consumption is very low, increasing
 486 it just slightly leads to massive accuracy gains. Then the curve has an in-
 487 flexion point, and the opposite becomes true: there is just a slight increase
 488 in accuracy when new or more costly features are added.

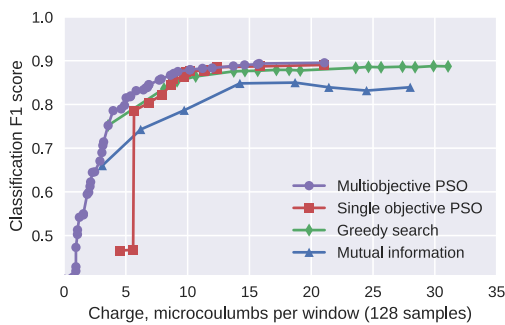


(a) Main dataset

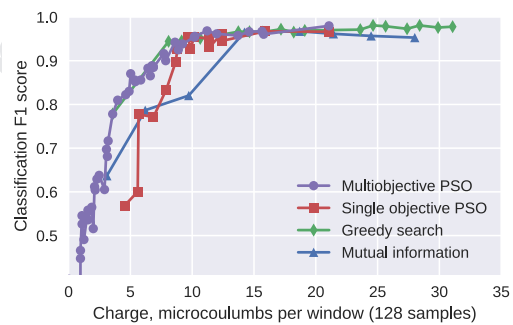


(b) Subject left out

Figure 6: Approximate Pareto-optimal fronts on the PAMAP2 dataset.

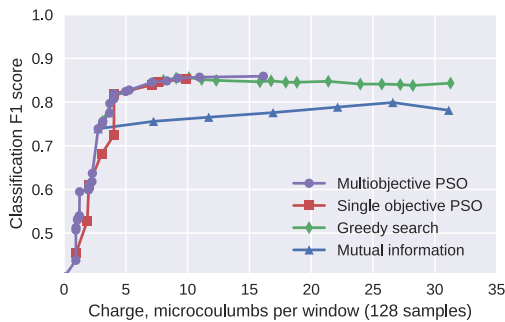


(a) Main dataset

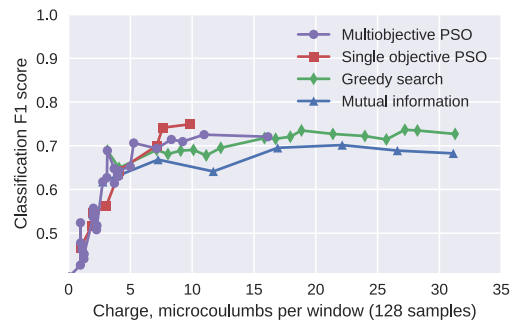


(b) Subject left out

Figure 7: Approximate Pareto-optimal fronts on the HAR dataset.



(a) Main dataset



(b) Subject left out

Figure 8: Approximate Pareto-optimal fronts on the SPHERE dataset.

489 *5.1. PSO Based Search*

490 The PSO methods show the best overall energy-accuracy tradeoff. The
 491 multi-objective shows slightly better results. However, its main benefit is that
 492 it obtains a higher number of solutions. The multi-objective PSO algorithm
 493 avoids crowding of particles, and as a result, it produces a Pareto-optimal
 494 front with higher granularity. The number of solutions it is consistently
 495 higher compared to the single objective PSO algorithm.

496 *5.2. Greedy Search*

497 The greedy search finds feature groups that are generally dominated by
 498 groups found by the PSO methods. Especially if saving energy is the main
 499 concern, the greedy search is not competitive. By its nature, the granularity
 500 of the results is low, since each iteration of the algorithm adds a new feature
 501 to the candidate set. However, the greedy search is faster to execute than
 502 the PSO methods.

503 *5.3. MI Based Selection*

504 This method performs significantly worse than the others. This is ex-
 505 plained as it is the only one that does not consider the energy cost in the
 506 selection process, and that it ignores the redundancy between different high-
 507 ranking features. Untypically, this method performs better on the test data
 508 than on validation data, for PAMAP2 and SPHERE datasets: unlike the
 509 other methods, this method does not fit the selected features to the valida-
 510 tion set.

511 *5.4. Dataset Specifics*

512 The PAMAP2 Dataset shows good match between the main dataset and
 513 the subject left out, and is the one that most benefits from the PSO methods.
 514 For the other datasets, the shape of the solution graph for the subject left
 515 out is slightly more different than the shape of the graph on the main portion
 516 of that dataset. The results on the SPHERE Challenge Dataset (Fig. 8) in
 517 particular are more affected by randomness, as it has fewer samples: it is an
 518 order of magnitude smaller than the other two datasets (Table 6).

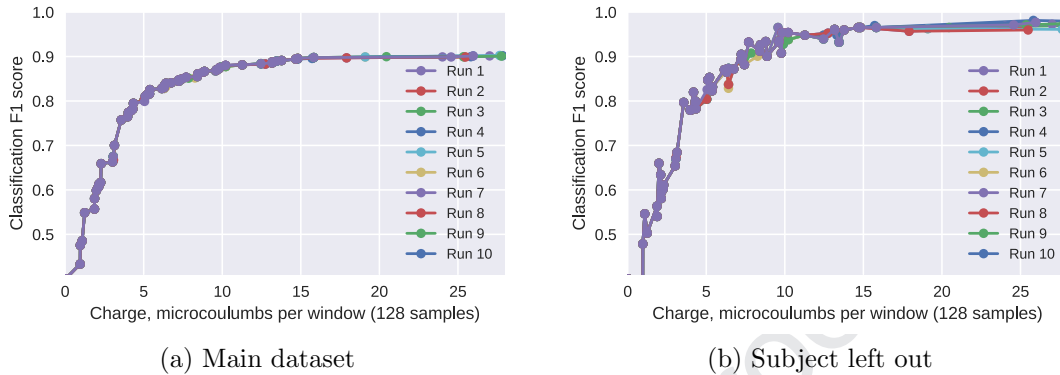


Figure 9: Results from repeated PSO multi-objective optimizations on the HAR dataset.

519 5.5. Repeatability

520 To investigate the repeatability of algorithms we select the best algorithm
 521 (PSO, multi-objective version) and run it on the HAR dataset 10 times.
 522 The results (Fig. 9) show that the initial selection of energy-efficient feature
 523 groups shows perfect repeatability, while high accuracy can be obtained in
 524 multiple different ways, so different groups are selected in the different runs.
 525 The results on the subject left out set show increased variability compared
 526 to the validation set, as the optimization process operates with the latter.

527 5.6. The Performance of Individual Features

528 Figures 10 and 11 show the most frequently occurring individual features.
 529 These figures exclude the results from the MI based search, as they were
 530 generally much worse than the other methods and did not take into account
 531 the energy cost.

532 The results show that there are no universally good features: no single
 533 feature shows up in all six different graphs. Each activity recognition ap-
 534 plication benefits from slightly different features. Furthermore, many of the
 535 features have high correlations with other features, therefore can be replaced
 536 with the other features at least for some of the applications. (It is worth
 537 noting that redundancy or very high correlation between features does not
 538 mean that they are always mutually replaceable [23].)

539 Figure 12 visualizes the frequency and energy consumption of individual
 540 features in the results, on all datasets and all algorithms, except the MI
 541 based search. *JerMagSq-iqr* is the only feature that shows up in five out

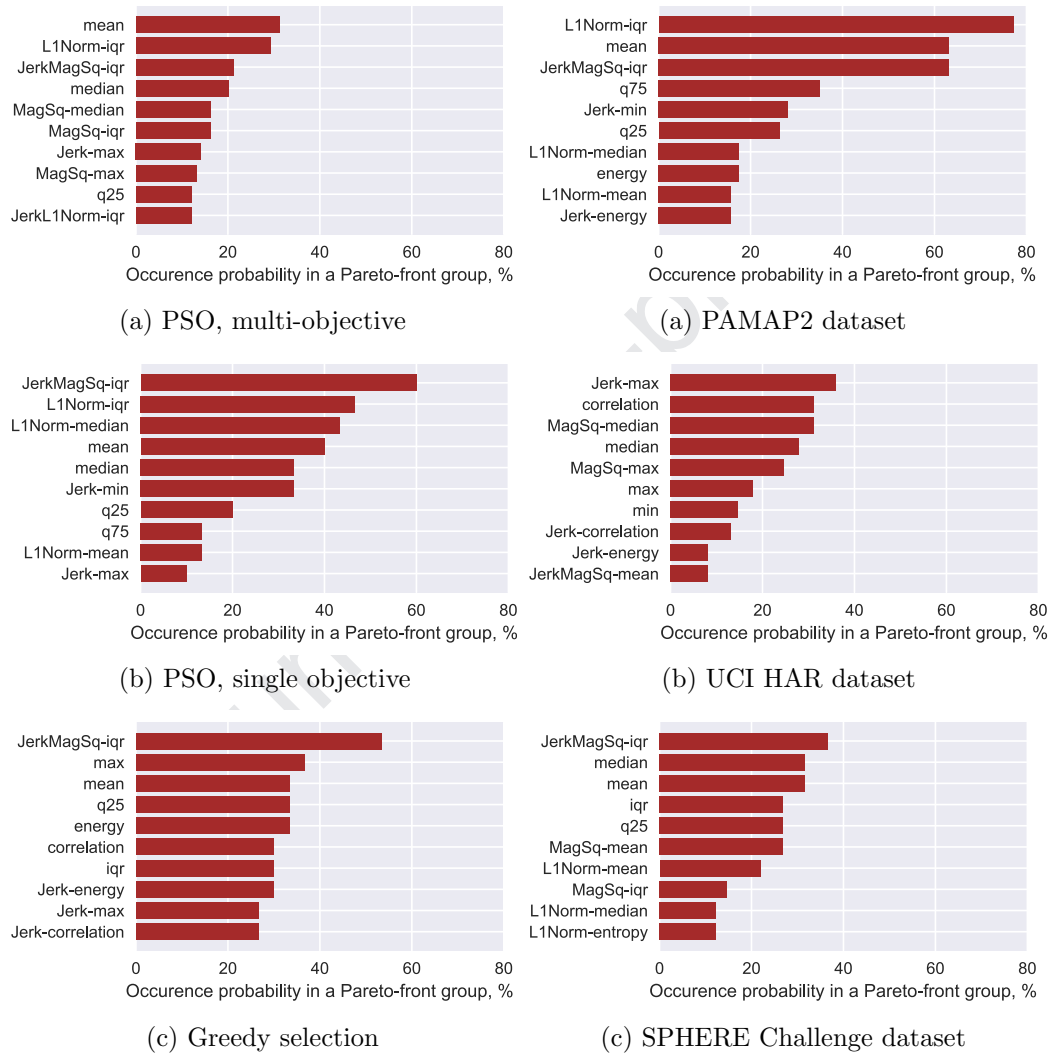


Figure 10: Ten most frequently occurring fea-

Figure 11: Ten most frequently occurring fea-
tures, plotted per dataset.

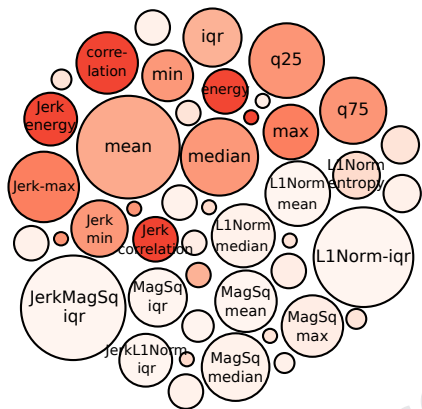


Figure 12: The energy consumption and the selection frequency of individual features. The diameter of the nodes is proportional to their frequencies in the results. The color of a node corresponds to its individual energy consumption (darker color – more energy).

542 of the six plots. It is likely that the main reason for that is how cheap
 543 it is to transmit the results of this feature. However, it would be rather
 544 difficult to manually come up with this feature, as it requires two intermediate
 545 transforms of the data (first *jerk*, then *magnitude squared*), succeeded by the
 546 calculation of both quartiles. We are not aware of any existing research that
 547 uses this particular feature. This demonstrates that our generalized approach
 548 of combining arbitrary transforms and calculating all candidate features on
 549 the result helps to discover novel, useful features.

550 5.7. Algorithm Runtime Performance

Table 7: Algorithm runtime performance on the SPHERE dataset.

Algorithm	Runtime, seconds
Mutual Information	4.6 s
Greedy search	454.2 s
PSO, multi-objective	1924.5 s
PSO, single objective	2413.6 s

551 The algorithms are envisioned to run offline, on a powerful computer. In
 552 Table 7 we provide results on an Lenovo Thinkpad X1 laptop with Intel Core
 553 i7-10710U CPU and 16 GB RAM. It can be seen the the mutual information

554 based method is by far the fastest one, while the wrapper search methods
 555 incur a significant runtime as they have to train and evaluate RF classifiers
 556 on the dataset many times over. The application only uses a single core of
 557 the CPU; there is a potential for several-fold improvement if multithreading
 558 or GPU were used. The exact performance depends both on the dataset size
 559 and the classifier parameters, such as the number of trees in the RF classifier
 560 (see Section 4.3).

561 6. Discussion

562 6.1. Energy Saved By Using the Feature Extraction

Table 8: F_1 score comparison with and without feature selection.

	PAMAP2 Dataset	HAR Dataset	SPHERE Challenge Dataset
F_1 score, best feature group	0.855	0.895	0.859
F_1 score, all features	0.854	0.833	0.820
Best F_1 score at $\leq 9.4 \mu C$	0.833	0.875	0.855

Table 9: Charge consumption comparison with and without feature selection.

	PAMAP2 Dataset	HAR Dataset	SPHERE Challenge Dataset
Raw data	94.38 μC	94.38 μC	94.38 μC
At 99 % of max F_1 score	20.02 μC	36.04 μC	36.24 μC
At 95 % of max F_1 score	8.39 μC	25.49 μC	36.08 μC
At 90 % of max F_1 score	6.55 μC	6.18 μC	7.128 μC

563 Wearable applications frequently collect the full acceleration data [39].
 564 Such an approach provides flexibility later on and is especially important if
 565 the initial hypothesis is not clear. However, simply adding more features
 566 may not improve the accuracy of the prediction (Table 8). When all features
 567 are used inputs to the RF classifier, the performance is worse in 5 cases out
 568 of 6 compared with selecting and sending over a group of features.

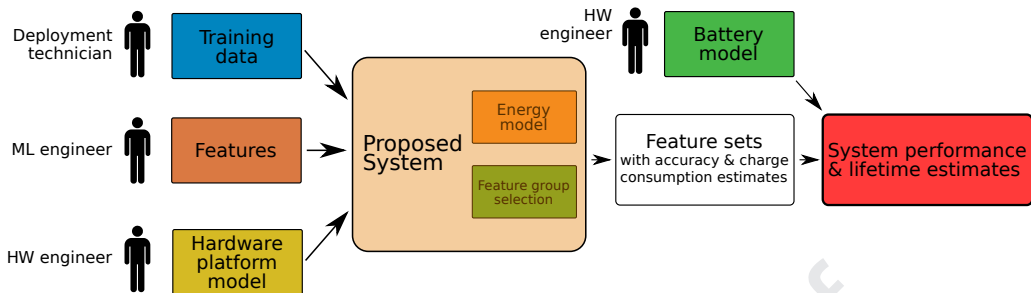


Figure 13: The envisioned application of the proposed system.

569 Moreover, the raw data transmission has much higher cost compared to
 570 extracting and transmitting features. On the target platform, collection raw
 571 data for a single window requires $31.46 \times 3 = 94.38 \mu\text{C}$ (Table 4). At 10%
 572 of that cost (i.e., at $\leq 9.4 \mu\text{C}$) the accuracy is similar to that obtained from
 573 using all features (Table 8). Hence, using the on-board feature extraction
 574 reduces the cost tenfold with only a small decrease in accuracy.

575 6.2. Application Examples

576 Fig. 13 shows the intended application of this work. The inputs of the
 577 proposed system are: labeled training data from a short-term pilot experi-
 578 ment, list of features, and the platform model. The amount of the training
 579 data required is not large: in our evaluation it ranges from 2.1 hours for
 580 SPHERE to >7 h for HAR (Table 6), although a more detailed activity pro-
 581 file may require more data. The amount of the data has an impact on the
 582 result quality (Figs. 6, 7, 8), but even for SPHERE it is acceptable.

583 The output is the approximate Pareto front of feature groups; it should
 584 be used together with a battery model that captures the discharge patterns
 585 of the hardware platform’s power source (its voltage and capacity dynamics
 586 under load). Given both, it is possible to answer questions about the accuracy
 587 and longevity of the deployments before actually carrying them out, thus
 588 saving time and effort.

589 **Example application 1.** *In a smart home project, wearable devices are*
 590 *to be deployed to participants together with recharging instructions. What*
 591 *is the minimum required recharge frequency, given that the system should*
 592 *achieve F_1 score ≥ 0.9 ?* Here, the question can be answered by collecting
 593 training data, running the feature group selection, and removing the results
 594 with $F_1 < 0.9$. The most efficient remaining feature set can be used, and the
 595 charge consumption can be translated to required recharge frequency using

596 a battery model.

597 **Example application 2.** *A clinical researcher plans to carry out a*
 598 *2-week trial with ill elderly people as the wearable users. What is the max-*
 599 *imum achievable F_1 score, given that the participants should not be required*
 600 *to recharge the devices?* Here, the charge consumption first must be trans-
 601 lated to battery life, and applied as a filter to the results; after that, the
 602 highest-scoring feature set provides the answer.

603 7. Conclusions

604 This paper proposes a framework for finding groups of features that have
 605 approximately optimal energy-accuracy trade-offs for activity recognition
 606 from acceleration data. The proposed system helps to answer questions about
 607 the expected battery lifetime and recognition accuracy of an activity recog-
 608 nition application without carrying a full-scale labor-intensive deployment.
 609 We describe a detailed energy consumption model that takes into account
 610 feature inter-dependencies and instantiate this model for an ARM Cortex-M3
 611 based wearable platform. Subsequently, we describe and evaluate a number
 612 of feature selection algorithms. Their evaluation using three datasets shows
 613 that the multi-objective Particle Swarm Optimization algorithm achieves the
 614 best results in terms of the accuracy-energy tradeoff. Extracting and send-
 615 ing the features requires an order of magnitude less energy compared with
 616 sending the raw data, while having minimal impact on the F_1 score.

617 Acknowledgments

618 This work was supported by the ERDF Activity 1.1.1.2 “Post-doctoral
 619 Research Aid” (No. 1.1.1.2/VIAA/2/18/282).

620 References

- 621 [1] J. Sengupta, S. Ruj, S. D. Bit, A Comprehensive survey on attacks,
 622 security issues and blockchain solutions for IoT and IIoT, *Journal of*
 623 *Network and Computer Applications* 149 (2020) 102481.
- 624 [2] W. Kassab, K. A. Darabkh, A–z survey of internet of things: Architec-
 625 tures, protocols, applications, recent advances, future directions and rec-
 626 ommendations, *Journal of Network and Computer Applications* (2020)
 627 102663.

- 628 [3] T. McGhin, K.-K. R. Choo, C. Z. Liu, D. He, Blockchain in healthcare
629 applications: Research challenges and opportunities, *Journal of Network
630 and Computer Applications* (2019).
- 631 [4] J. Qi, P. Yang, G. Min, O. Amft, F. Dong, L. Xu, Advanced Internet
632 of Things for personalised healthcare systems: A survey, *Pervasive and
633 Mobile Computing* 41 (2017) 132–149.
- 634 [5] A. Hadjidj, M. Souil, A. Bouabdallah, Y. Challal, H. Owen, Wireless
635 sensor networks for rehabilitation applications: Challenges and opportu-
636 nities, *Journal of Network and Computer Applications* 36 (2013) 1–15.
- 637 [6] A. Bajpai, V. Jilla, V. N. Tiwari, S. M. Venkatesan, R. Narayanan,
638 Quantifiable fitness tracking using wearable devices, in: *Engineering in
639 Medicine and Biology Society (EMBC), 2015 37th Annual International
640 Conference of the IEEE, IEEE*, pp. 1633–1637.
- 641 [7] P. Woznowski, A. Burrows, T. Diethe, et al., SPHERE: A Sensor Plat-
642 form for Healthcare in a Residential Environment, in: *Designing, De-
643 veloping, and Facilitating Smart Cities: Urban Design to IoT Solutions*,
644 Springer International Publishing, 2017, pp. 315–333.
- 645 [8] A. Elsts, R. McConville, X. Fafoutis, N. Twomey, R. Piechocki,
646 R. Santos-Rodriguez, I. Craddock, On-board feature extraction from
647 acceleration data for activity recognition, in: *Proceedings of the In-
648 ternational Conference on Embedded Wireless Systems and Networks
649 (EWSN)*.
- 650 [9] M. Janidarmian, A. Roshan Fekr, K. Radecka, Z. Zilic, A comprehensive
651 analysis on wearable acceleration sensors in human activity recognition,
652 *Sensors* 17 (2017) 529.
- 653 [10] N. Twomey, T. Diethe, X. Fafoutis, A. Elsts, R. McConville, P. Flach,
654 I. Craddock, A comprehensive study of activity recognition using ac-
655 celerometers, *Informatics* 5 (2018).
- 656 [11] U. Maurer, A. Smailagic, D. P. Siewiorek, M. Deisher, Activity recogni-
657 tion and monitoring using multiple sensors on different body positions,
658 in: *International Workshop on Wearable and Implantable Body Sensor
659 Networks (BSN), IEEE*.

- 660 [12] J. Wang, Y. Chen, S. Hao, X. Peng, L. Hu, Deep learning for sensor-
661 based activity recognition: A survey, *Pattern Recognition Letters*
662 (2018).
- 663 [13] C. Bormann, M. Ersue, A. Keranen, Terminology for Constrained-Node
664 Networks, RFC 7228, IETF, 2014.
- 665 [14] R. Possas, S. Pinto Caceres, F. Ramos, Egocentric activity recognition
666 on a budget, in: *Proceedings of the IEEE Conference on Computer*
667 *Vision and Pattern Recognition*, pp. 5967–5976.
- 668 [15] N. D. Lane, S. Bhattacharya, A. Mathur, P. Georgiev, C. Forlivesi,
669 F. Kawsar, Squeezing deep learning into mobile and embedded devices,
670 *IEEE Pervasive Computing* 16 (2017) 82–88.
- 671 [16] M. Satyanarayanan, The emergence of edge computing, *Computer* 50
672 (2017) 30–39.
- 673 [17] Z. Yan, V. Subbaraju, D. Chakraborty, A. Misra, K. Aberer, Energy-
674 efficient continuous activity recognition on mobile phones: An activity-
675 adaptive approach, in: *2012 16th international symposium on wearable*
676 *computers*, Ieee, pp. 17–24.
- 677 [18] D. Gordon, J. Czerny, T. Miyaki, M. Beigl, Energy-efficient activity
678 recognition using prediction, in: *2012 16th International Symposium on*
679 *Wearable Computers*, IEEE, pp. 29–36.
- 680 [19] Y. Liang, X. Zhou, Z. Yu, B. Guo, Energy-efficient motion related
681 activity recognition on mobile devices for pervasive healthcare, *Mobile*
682 *Networks and Applications* 19 (2014) 303–317.
- 683 [20] A. Elsts, Source node selection to increase the reliability of sensor net-
684 works for building automation, in: *EWSN*, pp. 125–136.
- 685 [21] L. Zheng, D. Wu, X. Ruan, S. Weng, A. Peng, B. Tang, H. Lu, H. Shi,
686 H. Zheng, A novel energy-efficient approach for human activity recog-
687 nition, *Sensors* 17 (2017) 2064.
- 688 [22] J. Miao, L. Niu, A survey on feature selection, *Procedia Computer*
689 *Science* 91 (2016) 919–926.

- 690 [23] I. Guyon, A. Elisseeff, An introduction to variable and feature selection,
691 Journal of machine learning research 3 (2003) 1157–1182.
- 692 [24] J. Kennedy, Particle swarm optimization, in: Encyclopedia of machine
693 learning, Springer, 2011, pp. 760–766.
- 694 [25] B. Xue, M. Zhang, W. N. Browne, Particle swarm optimization for
695 feature selection in classification: A multi-objective approach, IEEE
696 transactions on cybernetics 43 (2013) 1656–1671.
- 697 [26] N. Srinivas, K. Deb, Multiobjective optimization using nondominated
698 sorting in genetic algorithms, Evolutionary computation 2 (1994) 221–
699 248.
- 700 [27] R. Cilla, M. A. Patricio, A. Berlanga, J. M. Molina, Creating human
701 activity recognition systems using pareto-based multiobjective optimiza-
702 tion, in: 2009 Sixth IEEE International Conference on Advanced Video
703 and Signal Based Surveillance, IEEE, pp. 37–42.
- 704 [28] C. Emmanouilidis, A. Hunter, J. MacIntyre, A multiobjective evolu-
705 tionary setting for feature selection and a commonality-based crossover
706 operator, in: Proceedings of the 2000 Congress on Evolutionary Com-
707 putation. CEC00 (Cat. No. 00TH8512), volume 1, IEEE, pp. 309–316.
- 708 [29] N. Wang, G. V. Merrett, R. G. Maunder, A. Rogers, Energy and ac-
709 curacy trade-offs in accelerometry-based activity recognition, in: Com-
710 puter Communications and Networks (ICCCN), 2013 22nd International
711 Conference on, IEEE, pp. 1–6.
- 712 [30] D. Chu, N. D. Lane, T. T.-T. Lai, C. Pang, X. Meng, Q. Guo, F. Li,
713 F. Zhao, Balancing energy, latency and accuracy for mobile sensor data
714 classification, in: Proceedings of the 9th ACM Conference on Embedded
715 Networked Sensor Systems, ACM, pp. 54–67.
- 716 [31] U. Jensen, P. Kugler, M. Ring, B. M. Eskofier, Approaching the
717 accuracy–cost conflict in embedded classification system design, Pat-
718 tern Analysis and Applications 19 (2016) 839–855.
- 719 [32] X. Fafoutis, A. Vafeas, B. Janko, R. S. Sherratt, J. Pope, A. Elsts,
720 E. Mellios, G. Hilton, G. Oikonomou, R. Piechocki, I. Craddock, De-
721 signing Wearable Sensing Platforms for Healthcare in a Residential En-

- 722 vironment, EAI Endorsed Trans. Pervasive Health and Technology 17
723 (2017).
- 724 [33] C. Bormann, P. Hoffman, Concise Binary Object Representation
725 (CBOR), RFC 7049, IETF, 2013.
- 726 [34] J. Kennedy, Particle swarm optimization, in: Encyclopedia of machine
727 learning, Springer, 2011, pp. 760–766.
- 728 [35] A. Reiss, D. Stricker, Creating and benchmarking a new dataset for
729 physical activity monitoring, in: Proc. of the 5th Int. Conf. on Pervasive
730 Technologies Related to Assistive Environments, ACM, 2012, pp. 40:1–
731 40:8.
- 732 [36] D. Anguita, et al., A public domain dataset for human activity recog-
733 nition using smartphones, in: European Symp. on Artificial Neural
734 Networks, Computational Intell. and Mach. Learning (ESANN).
- 735 [37] N. Twomey, T. Diethe, M. Kull, H. Song, M. Camplani, S. Hannuna,
736 X. Fafoutis, et al., The SPHERE challenge: Activity recognition with
737 multimodal sensor data, arXiv preprint arXiv:1603.00797 (2016).
- 738 [38] N. Zhu, T. Diethe, M. Camplani, L. Tao, A. Burrows, N. Twomey,
739 D. Kaleshi, M. Mirmehdi, P. Flach, I. Craddock, Bridging e-Health and
740 the Internet of Things: The SPHERE project, IEEE Intelligent Systems
741 30 (2015) 39–46.
- 742 [39] A. Elsts, X. Fafoutis, P. Woznowski, E. Tonkin, G. Oikonomou,
743 R. Piechocki, I. Craddock, Enabling healthcare in smart homes: The
744 sphere iot network infrastructure, IEEE Communications Magazine 56
745 (2018) 164–170.

Author biographies

Atis Elsts received the Ph.D. degree in computer science from the University of Latvia, in 2014. He was with the Digital Health Engineering Group, University of Bristol, from 2016 to 2018, with the Swedish Institute of Computer Science (SICS), in 2015, and a Researcher with Uppsala University, from 2014 to 2015. Since December 2018, he has been a Researcher with the Institute of Electronics and Computer Science (EDI), Riga, Latvia. He is a maintainer of the Contiki-NG operating system for the Internet of Things (IoT). His scientific interests focus on experimental research in networked embedded Systems, including network protocols, wearable devices, and embedded machine learning.

Niall Twomey is a postdoctoral researcher on the Digital Health Engineering group at the University of Bristol. His research interests include data mining, fusion of environmental sensors in smart home environments, and the use of digital signal processing, machine learning, and application-centric decision making for objective health and wellness assessments. Twomey has a PhD in machine learning applied to signal processing from University College Cork, Ireland.

Ryan McConville is a Lecturer in Data Science, Machine Learning and AI within the Intelligent Systems Laboratory and Department of Engineering Mathematics at the University of Bristol. He gained his PhD working with the Centre for Secure Information Technologies (CSIT) at Queen's University Belfast in 2017 where he researched large scale unsupervised machine learning. His research interests lie around unsupervised machine learning with complex data.

Ian Craddock is currently a full professor with the University of Bristol, UK, and Director of the flagship "SPHERE" centre (www.irc-sphere.ac.uk) comprising approximately 100 researchers and clinicians working on IoT technology for health. He serves on the healthcare strategy board for the UK's largest engineering funder. He is also separately employed by Toshiba as Managing Director of their Telecommunications Research Lab in Bristol.

Conflict of Interest Statement

The authors declare no conflict of interest.

Journal Pre-proof